Manganese nanodepot augments host immune response against coronavirus

Yizhe Sun[1], Yue Yin[1], Lidong Gong[1], Zichao Liang[1], Chuanda Zhu[1], Caixia Ren[2], Nan Zheng[3], Qiang Zhang[4], Haibin Liu[5], Wei Liu[5], Fuping You[1], Dan Lu[1] (✉), and Zhiqiang Lin[1] (✉)

[1] Institute of Systems Biomedicine, Department of Pathology, School of Basic Medical Sciences, Beijing Key Laboratory of Tumor Systems Biology, Peking-Tsinghua Center for Life Sciences, Peking University Health Science Center, Beijing 100191, China
[2] Department of Human Anatomy, Histology and Embryology, Peking University Health Science Center, Beijing 100191, China
[3] Key Laboratory of Carcinogenesis and Translational Research (Ministry of Education/Beijing), National Drug Clinical Trial Center, Peking University Cancer Hospital & Institute, Beijing 100142, China
[4] Department of Pharmaceutics, School of Pharmaceutical Sciences, Peking University, Beijing 100191, China
[5] Department of General Surgery, Xinjiang Production and Construction Corps Hospital, Urumchi, Xinjiang Uygur Autonomous Region 830002, China

ABSTRACT

Interferon (IFN) responses are central to host defense against coronavirus and other virus infections. Manganese (Mn) is capable of inducing IFN production, but its applications are limited by nonspecific distributions and neurotoxicity. Here, we exploit chemical engineering strategy to fabricate a nanodepot of manganese (nanoMn) based on Mn^{2+}. Compared with free Mn^{2+}, nanoMn enhances cellular uptake and persistent release of Mn^{2+} in a pH-sensitive manner, thus strengthening IFN response and eliciting broad-spectrum antiviral effects in vitro and in vivo. Preferentially phagocytosed by macrophages, nanoMn promotes M1 macrophage polarization and recruits monocytes into inflammatory foci, eventually augmenting antiviral immunity and ameliorating coronavirus-induced tissue damage. Besides, nanoMn can also potentiate the development of virus-specific memory T cells and host adaptive immunity through facilitating antigen presentation, suggesting its potential as a vaccine adjuvant. Pharmacokinetic and safety evaluations uncover that nanoMn treatment hardly induces neuroinflammation through limiting neuronal accumulation of manganese. Therefore, nanoMn offers a simple, safe, and robust nanoparticle-based strategy against coronavirus.

KEYWORDS

interferon, coronavirus, manganese nanodepot (nanoMn), macrophage polarization, vaccine adjuvant

1 Introduction

The coronavirus disease 2019 (COVID-19) caused by severe acute respiratory syndrome coronavirus 2 (SARS-CoV-2) has spread rapidly and leads to global epidemic [1, 2]. Unfortunately, to date, no drug or vaccine has been validated to efficiently treat human coronavirus [3]. Therefore, it is an urgent need to develop a potent antiviral drug that can control or prevent the infection of coronavirus.

Similar to severe acute respiratory syndrome coronavirus (SARS-CoV) and Middle East respiratory syndrome coronavirus (MERS-CoV), SARS-CoV-2 is also an enveloped, positive-sense, single-stranded RNA beta-coronavirus [4]. However, unlike SARS-CoV or MERS-CoV, the entry receptor of SARS-CoV-2, angiotensin-converting enzyme 2 (ACE2), has species difference, which limits the establishment of mice models of SARS-CoV-2 [5]. As one member of subgroup 2a of beta-coronavirus, mouse hepatitis virus A59 (MHV-A59) is closely related to SARS-CoV and SARS-CoV-2, and acts as model coronavirus [6]. Previous studies have proved that MHV-A59 infection causes murine hepatitis, hypergammaglobulinemia and other pathologies with high mortality rate [7, 8]. This mouse model thus can benefit therapeutic studies of drugs or vaccines on coronavirus infection.

In contrast to SARS-CoV, SARS-CoV-2 is resistant to glucocorticoid therapy, triggering lower type-I-interferon (IFN) response [9]. Moreover, ex vivo studies reveal that SARS-CoV-2 is more susceptible to the treatment of IFNα or IFNβ than SARS-CoV [10, 11]. As the key role in innate immune response, type-I-IFN as well as its downstream IFN-stimulated genes (ISGs) elicit multiple-effects that restrict virus entry, viral replication and assembly as well as viral transmission [12]. Moreover, IFN stimulation augments antigen processing and presentation, which in turn facilitates T cell activation and expansion [12]. In addition to innate immunity, type-I-IFN is also involved in modulation of CD8+ T cell–mediated cellular immunity and humoral immunity [13]. Therefore, the limited type-I-IFN response induced by SARS-CoV-2 indicates that coronavirus has evolved an effective strategy to escape from immune attack.

Bivalent manganese ion has been reported to provoke type-I-IFN response through activating the cGAS-STING pathway [14]. However, direct administration of frequently-used manganese compounds like $MnCl_2$ would result in

unspecific distributions of Mn^{2+} *in vivo*, which limits its efficacy. Moreover, free manganese distributes easily into the brains and spinal cords, causing neurotoxicity [15, 16]. These defects greatly restrict direct application of Mn^{2+} as an immunotherapeutic agent *in vivo* [15]. As one of the main sources of type-I-IFN *in vivo*, macrophages play a crucial role in phagocytizing massive of nanoparticles injected into the body [17, 18]. To take full advantage of the above features for IFN responses, we have developed a non-toxic manganese nanodepot (nanoMn), which is composed of manganese phosphate core coated with asymmetric lipid bilayer and PEG hydration layer. In contrast to free Mn^{2+}, nanoMn are easily engulfed by macrophage, activating interferon signaling and polarizing M1 macrophage activation *in vivo*. Supplementation of nanoMn ameliorates coronavirus-induced tissue damage and improves the outcome of viral infection. In addition to the stimulatory role in innate immunity, nanoMn treatment can also promote the development of $CD8^+$ T cell memory and host adaptive immune response against coronavirus. We believe this nanoparticle is a promising antiviral drug and can be used to treat coronavirus infection.

2   Results

2.1   Coronavirus infection stimulates less type-I-IFN response

Recent research has shown that the coronavirus SARS-CoV-2 triggers lower interferon response and may have evolved to escape from immune attack [19]. To confirm the coronavirus-induced type-I-IFN levels for development of potential countermeasures, we employed murine coronavirus MHV-A59, a hepatic and neuronal tropic coronavirus, to infect C57BL/6 mice. Through analysis of the transcriptome of liver tissues, we found that, the type-I-IFN signaling was hardly activated during MHV-A59 infection, in contrast to upregulation of pro-inflammatory response. (Fig. 1(a), Fig. S1(a) in the Electronic Supplementary Material (ESM)). At the meanwhile, liver damage and suppression of multiple pathways related with metabolic process were also observed by gene set enrichment analysis (GSEA) of the RNA-seq data (Fig. 1(b), Fig. S1(b) in the ESM). Our data thus verify that coronavirus subverts immune surveillance, which leads to IFN unresponsiveness and exacerbates tissue damage.

2.2   Design of interferon-promoting manganese nano-depot

To provoke type-I-IFN response against coronavirus, we exploited chemical engineering strategy to fabricate a kind of controllable and uniform nanoMn based on Mn^{2+}, a cGAS-STING pathway-mediated IFN stimulator [14]. The nanoMn was prepared following two steps including water-in-oil (w/o) emulsion droplet-confined precipitation reaction and a film dispersion method (Fig. 1(c)). Structurally, nanoMn was composed of manganese phosphate core coated with asymmetric lipid bilayer and PEG hydration layer (Fig. 1(c)). NanoMn was a multi-component system including manganese phosphate, 1,2-dioleoyl-sn-glycero-3-phosphate (DOPA), 1,2-dioleoyl-3-trimethylammonium-propane (DOTAP), cholesterol, and 1,2-distearoyl-sn-glycero-3-phosphoethanolamine-N-[methoxy (polyethylene glycol)-2000] (DSPE-PEG) with the molar ratio of 75:55:10:10:3. Following our preparation technology, the Mn^{2+} loading level was 0.44 g/kg (weight of manganese in total system), sufficient for administrated dose *in vivo*. This method resulted in high yield of 85.3% calculated by the manganese

levels. Using negative staining followed by transmission electronic microscope (TEM), both the manganese phosphate core and lipid coating layers of nanoMn were clearly visible (Fig. 1(d)). NanoMn were hollow spherical nanoparticles with size of about 20–30 nm, a little smaller than that determined by dynamic light scattering (DLS) method (average size of 35 nm), mainly due to the influence of PEG hydration layer (Figs. 1(d) and 1(e)). Zeta potential of nanoMn was +17.9 mV, obviously different from the control nanoparticles with the outer leaflet lipid of DOPA (–60.1 mV) or DOTAP (+31.7 mV), illustrating formation of asymmetrical lipid bilayers (Fig. 1(f)). As shown in Fig. 1(g), nanoMn persistently released Mn^{2+} in a pH-dependent manner. The percentage of cumulative Mn^{2+} release from nanoMn in pH 4.5 and 6.5 was much higher than that in pH 7.4 (89.07% in pH 4.5 vs. 35.92% in pH 7.4 at the timepoint of 24 h), suggesting that nanoMn could maintain a stable nanostructure in extracellular microenvironment but release Mn^{2+} fast in intracellular endosome (pH 5.0–6.5) and lysosome (pH 4.0–4.5).

To characterize the cellular uptake efficiency of nanoMn and its IFN-stimulatory effect, we treated bone marrow derived macrophages (BMDMs) with nanoMn or $MnCl_2$. As shown in Fig. 1(h), compared with $MnCl_2$ treatment, higher intracellular concentrations of manganese ions were detected in cells treated with nanoMn. Notably, the saturating concentrations of Mn^{2+} were also increased by nanoMn as relative to $MnCl_2$ did (Fig. 1(h)). Accordingly, the nanoMn treatment stimulated stronger type-I-IFN response in BMDMs (Fig. 1(i), Figs. S1(c)–S1(f) in the ESM).

2.3   NanoMn elicits potent and broad-spectrum antiviral effects

To explore whether stimulatory effects on IFN signaling by nanoMn can limit viral replication, we used green fluorescent protein-expressing vesicular stomatitis virus (VSV-GFP) to infect Hela cells in presence of nanoMn, $MnCl_2$, or vehicle control, respectively. Compared with free Mn^{2+} ($EC_{50} = 71.67$ μM), the treatment of nanoMn elicited stronger effects on suppression of viral replication ($EC_{50} = 3.897$ μM) (Figs. 2(a) and 2(b)). To determine whether nanoMn treatment can restrain the infection of other viruses, we used MHV-A59, Herpes simplex virus (HSV) or lymphocytic choriomeningitis virus (LCMV) to infect Hela cells. As shown in Figs. 2(c)–2(g), nanoMn treatment elicited broad-spectrum antiviral effects as compared with vehicle control did. Accordingly, the antiviral effects of nanoMn were obviously stronger than $MnCl_2$ did (Figs. 2(c)–2(g)). To determine whether the antiviral effects of nanoMn depend on type-I-IFN, we induced BMDMs from wild-type (WT) and $Irf3^{-/-}$ C57BL/6 mice (Fig. S2(a) in the ESM). Since interferon regulatory factor 3 (IRF3) is a downstream transcriptional factor of IFN signaling, knockout of IRF3 impaired type-I-IFN production [20]. Consistently, we found that nanoMn or $MnCl_2$ treatment hardly induced production of IFNβ in $Irf3^{-/-}$ BMDMs compared with WT cells (Fig. 2(h)). Subsequently, we collected the culture mediums of WT and $Irf3^{-/-}$ BMDMs treated with nanoMn or $MnCl_2$ for culturing HeLa cells, followed by viral infection. As shown in Fig. 2(i), culture mediums from WT mice treated with nanoMn significantly limited replication of MHV-A59, while deletion of IRF3 completely abolished this effect. Similar results were also observed upon VSV-GFP infection (Figs. S2(b) and S2(c) in the ESM). Our data thus identify that nanoMn has potent and broad-spectrum antiviral effects through modulating type-I-IFN production.
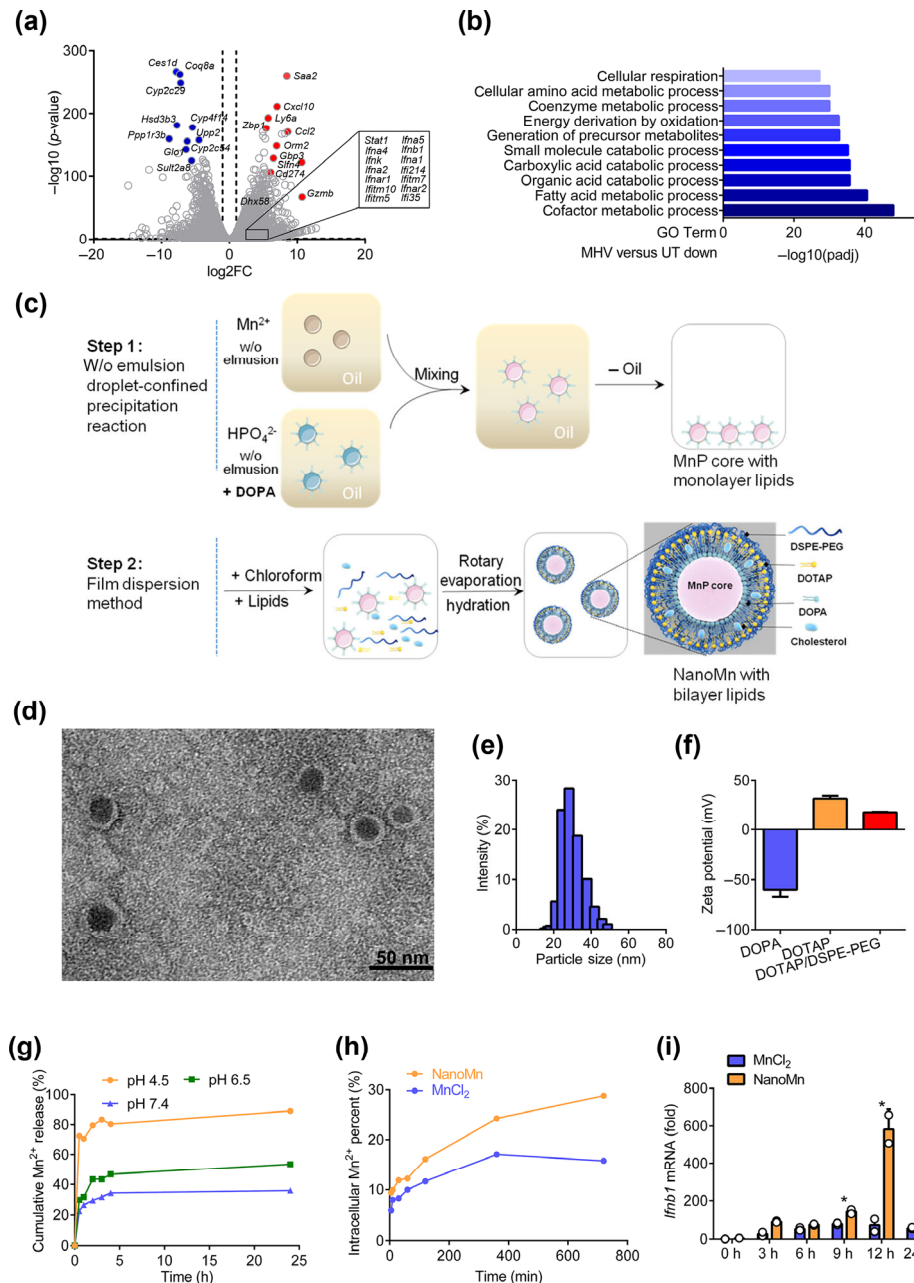
Figure 1 Preparation and characterization of manganese nanodepot for treatment of coronavirus infection. (a) C57BL/6 mice were untreated or intraperitoneal infected with 3×10^5 PFU MHV-A59. On day 4 post infection, livers of the mice were harvested, and subjected to RNA-seq assay. The differentially expressed genes were showed by the volcano plot. The up-regulated genes in infected mice were marked in red, while down-regulated genes were in blue. Genes encoding type-I-IFNs and ISGs which have no significant difference were indicated in the box. FC, fold change. (b) Transcriptomic analysis of gene expression in livers from control mice vs. mice that infected with 3×10^5 PFU MHV-A59 for 4 days. The differentially expressed genes that were down-regulated in the infected mice were used for enrichment analysis with GO database. UT, untreatment. (c) Schematic diagram of nanoMn preparation method. NanoMn was fabricated following two steps. The first step was performed by a method w/o emulsion droplet-confined precipitation reaction in order to obtain MnP core with a single layer of lipid, DOPA. The second step was carried out by a film dispersion method to coat outer leaflet lipid of DOTAP and DSPE-PEG onto MnP core for nanoMn. (d) Representative TEM image of negative stained nanoMn. NanoMn is a hollow spherical nanoparticle with a size of about 20–30 nm. Scale bar: 50 nm. (e) Particle size of nanoMn determined by DLS methods at the temperature of 25 °C. (f) Zeta potential of nanoMn assayed by a PSS ZPW388-NICOMP Particle Sizing System. The formulations with various outer leaflet lipid of DOPA, DOTAP, and DOTAP/DSPE-PEG (nanoMn) were prepared in order to investigate the effect of lipid materials on the surface charge of nanoMn. (g) Mn^{2+} Release from nanoMn lyophilized powders in PBS medium with different pH values at 4.5, 6.5, and 7.4. NanoMn persistently released Mn^{2+} in a pH-dependent manner. (h) BMDMs were treated with 10 μM $MnCl_2$ or nanoMn for indicated minutes. Cells and culture mediums were collected, and subjected to ICP-MS assay. For each time point, Mn^{2+} concentration in untreated cells and culture mediums were subtracted, and the proportions of intracellular Mn^{2+} to total Mn^{2+} were used for plotting. (i) BMDMs from C57BL/6 mice were treated with 10 μM $MnCl_2$ or nanoMn for indicated hours. Expression levels of *Ifnb1* in the cells were determined by qRT-PCR analysis ($n = 2$ cell cultures, mean ± standard deviation (SD); *$p < 0.05$). Statistical significance was assessed by two-tailed unpaired Student's *t*-test (i). (d)–(g), and (i) Data are representative of two independent experiments. See also Fig. S1 in the ESM.

2.4 NanoMn treatment strengthens host antiviral immune response *in vivo*

To further determine the antiviral effects of nanoMn *in vivo*,

we sequentially injected manganese formulations and the lethal dose of MHV-A59 with 24-h interval into the peritoneal cavity of C57BL/6 mice. As shown in Fig. 3(a), although $MnCl_2$ treatment prolonged the survival time of virus-infected mice
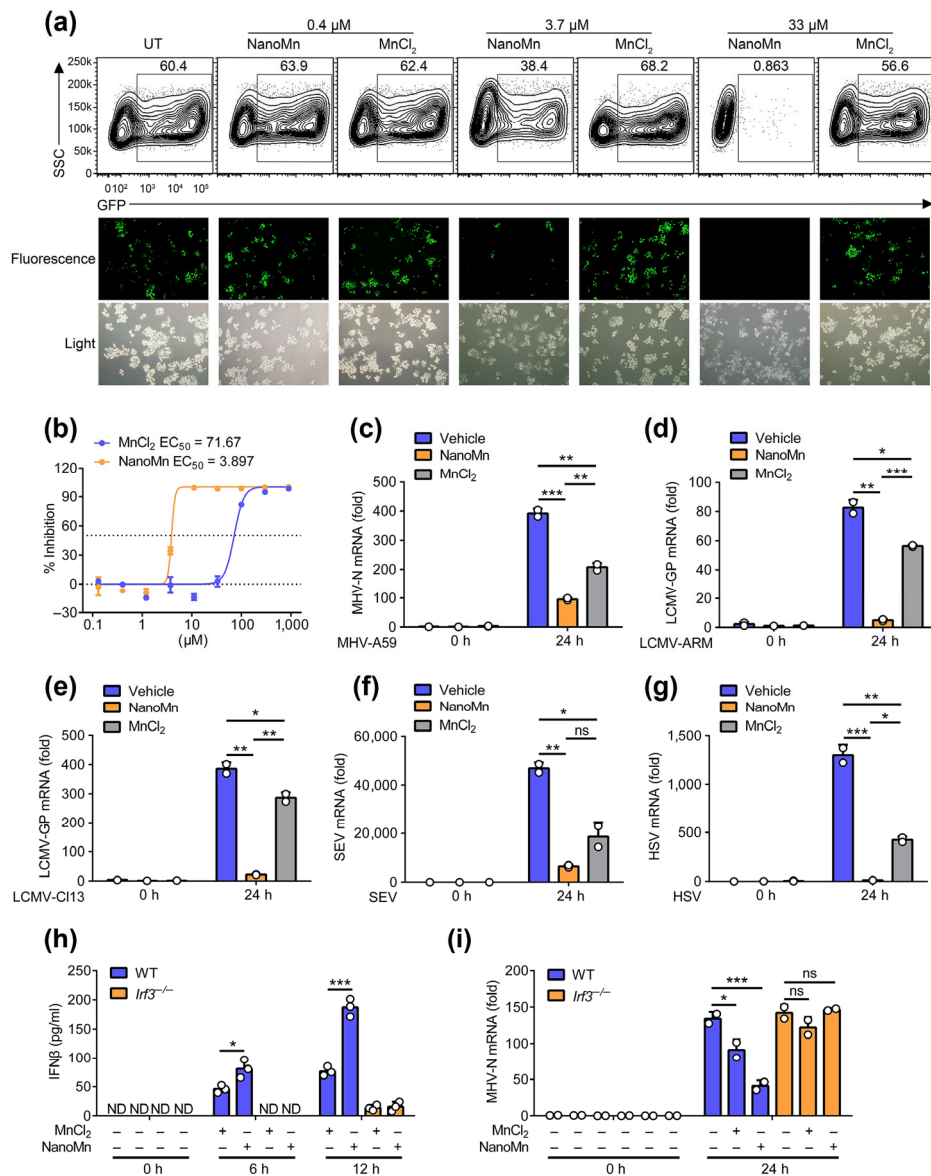
Figure 2 NanoMn elicits potent and broad-spectrum antiviral effects. (a) and (b) HeLa cells were treated with different concentrations of $MnCl_2$ or nanoMn, and infected with 0.01 MOI VSV-GFP for 16 h. The cells were subjected to microscopy analysis and flow cytometry analysis (a), and the percentages of GFP positive cells relative to untreatment control were used for calculation of EC_{50} (b). UT, untreatment. (c)–(g) HeLa cells were treated with 10 μM $MnCl_2$, nanoMn, or PBS (vehicle, as negative control). In the meantime, cells were infected with 0.01 MOI indicated virus for 24 h. Expression levels of viral RNAs were determined by qRT-PCR analysis ($n = 2$ cell cultures, mean ± SD; ns, not significant; $*p < 0.05$, $**p < 0.01$, $***p < 0.001$). (h) BMDMs induced from WT and $Irf3^{-/-}$ mice were treated with 10 μM $MnCl_2$ or nanoMn for indicated hours, and the culture mediums were collected. Production of IFNβ was determined by ELISA ($n = 3$ cell cultures, mean ± SD; $*p = 0.0237$, $***p = 0.0004$). ND, not detected. (i) BMDMs induced from WT and $Irf3^{-/-}$ mice were treated with 10 μM $MnCl_2$ or nanoMn for 10 h, and the culture mediums were collected. HeLa cells were pre-treated with the culture mediums for 1 h, followed by infection with 0.01 MOI MHV-A59. Expression levels of RNA of MHV-N gene were determined by qRT-PCR analysis ($n = 2$ cell cultures, mean ± SD; ns, not significant; $*p = 0.0167$, $***p = 0.0003$). EC_{50} was calculated using log (inhibitor) vs. normalized response (variable slope by Prism GraphPad software v6.01 (b)). (c)–(g), and (i) Statistical significance was assessed by one- or two-way ANOVA followed by Tukey's multiple comparisons test, or two-tailed unpaired Student's *t*-test (h). (a)–(g), and (i) Data are representative of two independent experiments. See also Fig. S2 in the ESM.

to some extent, all mice treated with vehicle or $MnCl_2$ died within 8 days post viral infection. Notably, a half of nanoMn-pretreated mice survived in this process (Fig. 3(a)). Through gross tissue examination, ecchymosis spots were detected in livers injected with vehicle or $MnCl_2$, rather than nanoMn (Fig. 3(b)). Using hematotylin and eosin (H&E) staining, large areas of necrosis and massive lymphocytes infiltration were induced by MHV infection, which were ameliorated and disseminated by the nanoMn treatment as compared with vehicle or $MnCl_2$ did (Fig. 3(c)). Moreover, quantitative real-time polymerase chain reaction (qRT-PCR) assays revealed that nanoMn treatment remarkably reduced the viral titrations in liver and spleen (Fig. 3(d)). Our data thus demonstrate that

nanoMn-induced immune responses can improve the outcome of coronavirus infection.

To explore the mechanism by which nanoMn restricts viral infection, we analyzed the peritoneal immune cells from the C57BL/6 mice pretreated with intraperitoneal injection of nanoMn or $MnCl_2$. In spite of the comparable numbers of lymphoid cells ($CD3^+$ or $B220^+$) and neutrophils ($CD11b^+$ $F4/80^-$ $Gr1^{hi}$) (Fig. 3(e), Figs. S3(a) and S3(b) in the ESM), the numbers of total immune cells ($CD45^+$) were increased by nanoMn treatment (Figs. 3(e) and 3(f)). Further analysis of myeloid cells revealed that the percentages and numbers of macrophages ($CD11b^+$ $F4/80^+$) were significantly increased post nanoMn treatment as relative to vehicle or $MnCl_2$
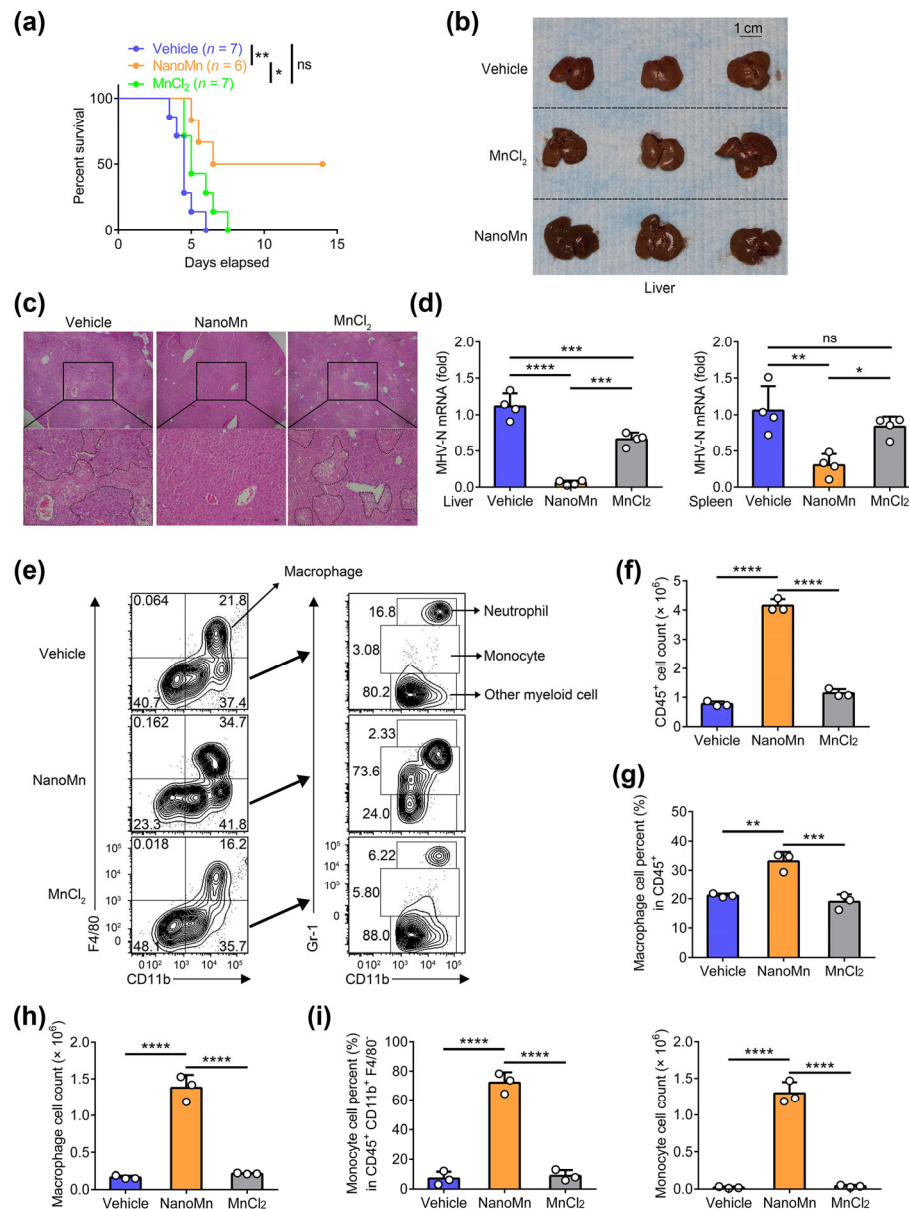
Figure 3 NanoMn treatment strengthens host antiviral immune response *in vivo*. (a)–(d) C57BL/6 mice were pretreated with 12 μmol/kg (660 μg/kg Mn^{2+}) $MnCl_2$, nanoMn, or PBS (vehicle) through intraperitoneal injection. 24 h later, mice were i.p. infected with 3×10^5 PFU MHV-A59. (a) The mice were monitored for survival over time (vehicle, $n = 7$ mice; nanoMn, $n = 6$ mice; $MnCl_2$, $n = 7$ mice: ns, not significant: $^*p = 0.0486$, $^{**}p = 0.0044$). (b) and (c) On day 4 post infection, livers of the infected mice were collected, and used for gross examination (b) and H&E staining (c). The dotted line indicates the necrotic area. (d) On day 4 post infection, the mice were sacrificed, and the spleens and livers were harvested. Expression levels of MHV-N gene were determined by qRT-PCR assay ($n = 4$ mice, mean ± SD; ns, not significant; $^*p = 0.0214$, $^{**}p = 0.0028$, $^{***}p < 0.001$, $^{****}P < 0.0001$). (e)–(i) C57BL/6 mice were i.p. injected with 12 μmol/kg (660 μg/kg Mn^{2+}) $MnCl_2$, nanoMn, or PBS (vehicle). Twelve hours later, the cells in the peritoneal cavity were isolated and counted, using for flow cytometry analysis (e). Absolute cell number of $CD45^+$ immune cell was calculated and used for statistical analysis (f). Percentages and cell count of macrophage ($CD11b^+$ $F4/80^+$) and monocyte ($CD11b^+$ $F4/80^-$ $Gr1^{lo}$) were used for statistical analysis (g)–(i) ($n = 3$ mice, mean ± SD; $^{**}p = 0.0021$, $^{***}p = 0.0009$, $^{****}p < 0.0001$). Statistical significance was assessed by log-rank (Mantel–Cox) test (a) or one-way ANOVA followed by Tukey's multiple comparisons test (d), (f)–(i). Data are representative of two independent experiments (b)–(i) or pooled from two independent experiments (a). See also Fig. S3 in the ESM.

treatment (Figs. 3(g) and 3(h)). Moreover, nanoMn treatment induced massive monocytes ($CD11b^+$ $F4/80^-$ $Gr1^{lo}$) accumulation in the peritoneal cavity (Fig. 3(i)), which would terminally differentiate into macrophages. Our data thus demonstrate that nanoMn treatment stimulates host antiviral immune response and limits coronavirus infection *in vivo*.

2.5 NanoMn drives M1 macrophage polarization and type-I-IFN production

As foreign substances, nanoparticles are mainly phagocytized by macrophages after entering the body [18]. To investigate the transportation efficiency and immunostimulatory effect of

nanoMn in macrophages, we isolated the peritoneal macrophages (PMs) from C57BL/6 mice post injection of nanoMn or $MnCl_2$. In accordance with *in vitro* data that nanoMn treatment increased intracellular concentration of Mn^{2+}, higher concentration of Mn^{2+} was detected in PMs treated with nanoMn as relative to $MnCl_2$ (Fig. 4(a)). Accordingly, higher expression levels of genes associated with type-I-IFN signaling were observed in PMs from nanoMn treated mice than those treated with $MnCl_2$ (Figs. 4(b)–4(d)).

Rather than alternatively activated or M2 macrophages, interferons are mainly produced by M1 macrophages, which are more conducive to viral clearance [21]. To determine whether
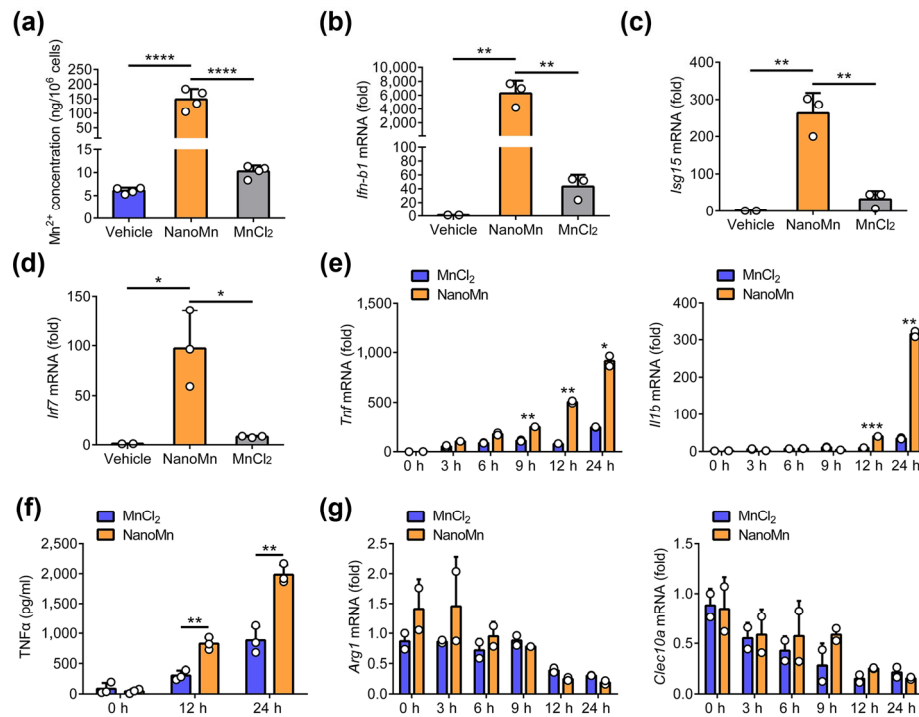
Figure 4 NanoMn drives M1 macrophages polarization and type-I-IFN production. (a)–(d) C57BL/6 mice were i.p. injected with 12 μmol/kg (660 μg/kg Mn^{2+}) $MnCl_2$, nanoMn, or PBS (vehicle). Twelve hours post injection, the peritoneal macrophages were isolated and counted, using for ICP-MS assay (a) ($n = 4$ mice, mean ± SD; ****$P < 0.0001$). Expression levels of indicated genes were assessed by qRT-PCR analysis (b)–(d) (vehicle, $n = 2$ mice; nanoMn or $MnCl_2$, $n = 3$ mice, mean ± SD; *$p < 0.05$, **$p < 0.01$). (e)–(g) BMDMs from C57BL/6 mice were treated with 10 μM $MnCl_2$ or nanoMn for indicated hours. Expression levels of indicated genes were determined using qRT-PCR analysis (e) and (g) ($n = 2$ cell cultures, mean ± SD; *$p < 0.05$, **$p < 0.01$, ***$p < 0.001$). Production of TNFα was determined by ELISA (f) ($n = 3$ cell cultures, mean ± SD; **$p < 0.01$). Statistical significance was assessed by one-way ANOVA followed by Tukey's multiple comparisons test (a)–(d) or two-tailed unpaired Student's t-test (e) and (f). (b)–(e), and (g) Data are representative of two independent experiments.

nanoMn treatment affects macrophage polarization, we treated BMDMs with nanoMn or $MnCl_2$. Interestingly, expression of genes characteristic of activated M1 macrophage (*Il1b* and *Tnf*) and production of TNFα protein were upregulated upon nanoMn treatment, while expression levels of genes involved in M2 macrophage activation (*Arg1* and *Clec10a*) were decreased (Figs. 4(e)–4(g)). Taken together, our results uncover that nanoMn promotes M1 macrophage polarization, which in turn enhances interferon-mediated viral suppression.

2.6 NanoMn ameliorates coronavirus-induced tissue damage

To evaluate the therapeutic benefits of nanoMn, we first developed virus-infected C57BL/6 mouse models by intraperitoneal injection of lethal dosage of MHV-A59. The diseased mice were then received therapeutic regime with nanoMn, $MnCl_2$, or vehicle, respectively (Fig. 5(a)). As expected, we found that nanoMn significantly prolonged the survival time of infectious mice, while other mice treated with vehicle or $MnCl_2$ died within 7 days post viral infection (Fig. 5(b)). Ensued gross tissue evaluation and histological analysis further confirmed these results (Figs. 5(c) and 5(d)). Accordingly, compared with mice treated with vehicle or $MnCl_2$, nanoMn treatment limited viral propagation in liver and spleen (Fig. 5(e)). To comprehensively analyze the therapeutic effects of nanoMn on coronavirus infection, we performed RNA-seq assay to analyze the differentially expressed genes in liver tissues during viral infection. Compared with mice treated with vehicle or $MnCl_2$, nanoMn rescued the expression of genes from pathways associated with metabolism process, which were influenced by coronavirus infection (Figs. 5(f) and 5(g)). Moreover, we also noticed that nanoMn treatment resulted in mild spleen enlargement and

greater amount of splenocytes (Figs. 5(h) and 5(i)), indicating that host adaptive immunity was also involved in nanoMn-mediated antiviral response. Our data thus demonstrate that nanoMn treatment can improve the outcome of coronavirus diseases.

2.7 NanoMn acts as a vaccine adjuvant to boost host adaptive immunity

In addition to pro-inflammatory cytokine production, M1 macrophage is also substantial for antigen presentation, which in turn stimulates expansion of an allogeneic T cell population [21]. To assess the role of nanoMn in modulation of host adaptive immunity, we first infected C57BL/6 mice with non-lethal dose of coronavirus with or without nanoMn. Two weeks post primary viral infection, we then re-challenged mice with lethal dose of MHV-A59 (Fig. S4(a) in the ESM). As shown in Fig. S4(b) in the ESM, all virus re-challenged mice survived. Moreover, qRT-PCR assays revealed that, compared with primary virus-infected mice, the viral titrations in virus re-challenged mice were significantly decreased (Fig. S4(c) in the ESM).

We next assessed the T cell development on day 7 post non-lethal dose viral infection. As shown in Fig. S4(d) in the ESM, nanoMn treatment facilitated the polarization of $CD8^+$ memory T cell ($CD44^{hi}$ $CD62L^+$) in liver and spleen. To further confirm the stimulatory role of nanoMn in memory T cell function, we employed lethal dose of MHV-A59 to re-challenge virus-infected mice in presence or absence of nanoMn treatment. On day 3 post re-infection of MHV-A59, more $CD8^+$ $CD25^+$ (activated) T cells but less $CD4^+$ $CD25^+$ (regulatory) T cells were detected in liver from mice treated with nanoMn (Fig. S4(e) in the ESM). In accordance with the T cell polarization results, nanoMn treatment resulted in greater amount of
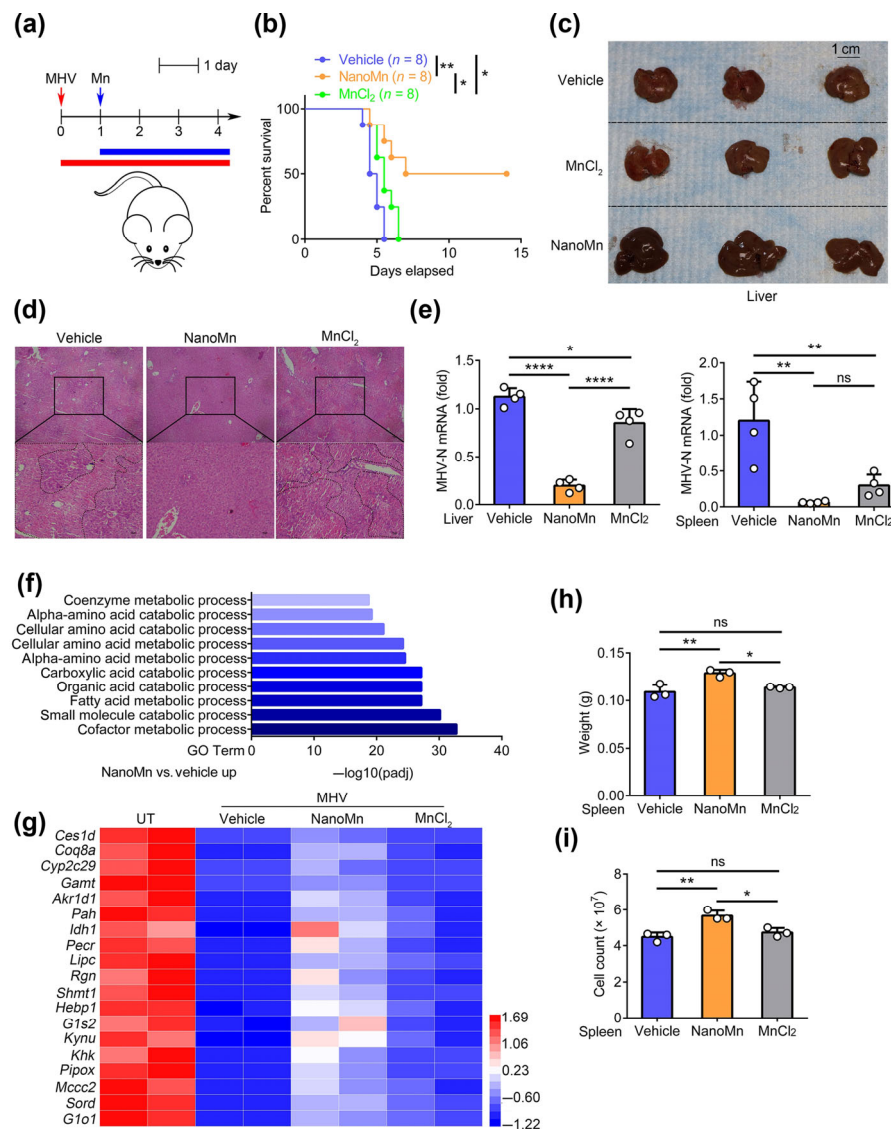
Figure 5 NanoMn ameliorates coronavirus-induced tissue damage. (a)–(i) C57BL/6 mice were i.p. infected with 3×10^5 PFU MHV-A59. 24 hours later, mice were i.p. injected with 12 µmol/kg (660 µg/kg Mn^{2+}) $MnCl_2$, nanoMn, or PBS (vehicle). (a) A graphic model of mice treatment. (b) Survival rates of the mice were monitored over time ($n = 8$ mice, *$p < 0.05$, **$p = 0.0018$).(c) and (d) Gross examination (c) and H&E staining (d) of the livers of the infected mice on day 4 post infection. The dotted line indicates the necrotic area. (e) On day 4 post infection, the organs of the infected mice were collected, and the expression levels of MHV-N gene in the organs were assessed by qRT-PCR assay ($n = 4$ mice, mean ± SD; ns, not significant; *$p = 0.0137$, **$p < 0.01$, ****$p < 0.0001$). (f) and (g) The livers of the infected mice were harvested on day 4 post infection, and used for RNA-seq assay. The differentially expressed genes that were up-regulated in the mice treated with nanoMn vs. vehicle were used for enrichment analysis with GO database (f). Expression levels of metabolism related genes of untreated or infected mice were showed in the heatmap (g). UT, untreatment. (h) and (i) On day 4 post infection, the spleens of the infected mice were collected and weighted (h). The lymphocytes in the spleens were isolated and counted, using for the statistical analysis (i) ($n = 3$ mice, mean ± SD; ns, not significant; *$p < 0.05$, **$p < 0.01$). Statistical significance was assessed by log-rank (Mantel–Cox) test (b) or one-way ANOVA followed by Tukey's multiple comparisons test (e), (h), and (i). Data are representative of two independent experiments (c)–(e), (h)–(i) or pooled from two independent experiments (b).

effector cytokines (TNFα⁺ IFNγ⁺) produced by T cells in liver (Fig. S4(f) in the ESM). Together, these results indicate that nanoMn treatment enhances cellular immune response against coronavirus.

The promotion effects of nanoMn on adaptive immunity make it a possible vaccine adjuvant. To this end, we used inactive LCMV virus in the presence or absence of nanoMn to immunize C57 mice, thus investigating the effect of nanoMn on antigen-specific T cell. As expected, we found that immunization with nanoMn resulted in spleen enlargement and greater amount of splenocytes (Figs. 6(a)–6(c)). More importantly, using tetramer staining, we found that nanoMn treatment promoted the production of antigen-specific T cell (Fig. 6(d)). Analogue to these results, GP₃₃₋₄₁ peptide treatment induced significant higher amount of effector cytokines produced by these T cells (Fig. 6(e)).

To further determine whether nanoMn affects humoral immunity, we immunized C57BL/6 mice with low dose of MHV-A59 in presence or absence of nanoMn through sub-cutaneous injection (Fig. 6(f)). Similar to the intraperitoneal injection, all immunized mice were survived when re-challenging with lethal dose of MHV-A59 on day 14 post primary viral infection. As shown in Fig. 6(g), nanoMn treatment increased the serum IgG concentration as relative to control mice. Taken together, our data demonstrate that nanoMn can function as a vaccine adjuvant to boost adaptive immunity and protect host from coronavirus infection.

2.8 NanoMn shows superior safety *in vivo*

Despite the essential role in antiviral immunity, excess of manganese is harmful to the central nervous system (CNS) due to the preferential uptake of Manganese by the brain [15].
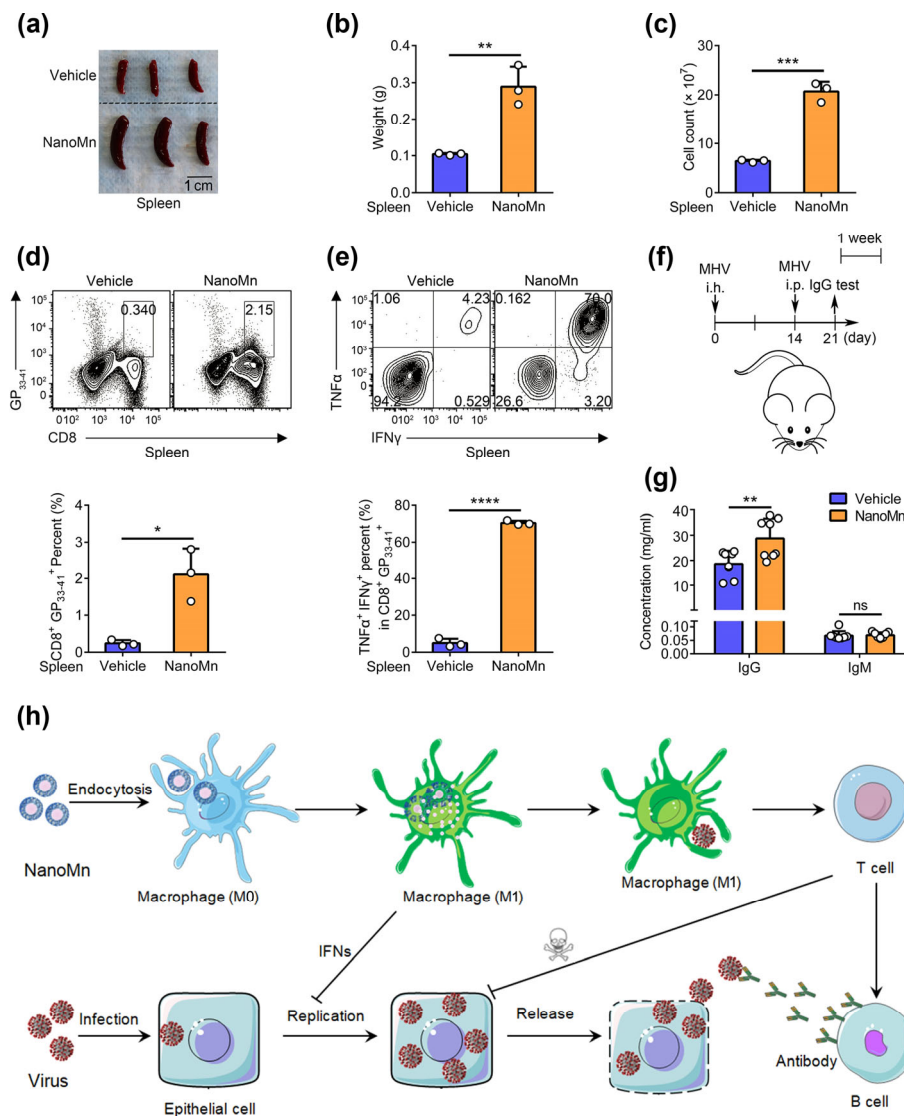
Figure 6 NanoMn acts as a vaccine adjuvant to boost host adaptive immunity. (a)–(e) 1×10^5 PFU LCMV-Cl13 were inactivated by heating at 54 °C for 30 min. C57BL/6 mice were subcutaneous injected with the inactive virus in the presence or absence of 0.24 μmol (13.2 μg of Mn^{2+}) nanoMn. (a)–(c) 10 days post inoculation, spleens were harvested from the mice for photographing (a) and weighing (b). Splenocytes were isolated and counted (c) ($n = 3$ mice, mean ± SD; **$p = 0.0040$, ***$p = 0.0002$). (d) The splenocytes were stained with tetramer, and percentages of $CD8^+$ GP_{33-41}^+ cells were assessed by flow cytometry analysis ($n = 3$ mice, mean ± SD; *$p = 0.0109$). (e) The cells were treated with 2 μg/ml GP_{33-41} peptide for 5 h, and the production of TNFα and IFNγ in the $CD8^+$ GP_{33-41}^+ cells were assessed by flow cytometry analysis ($n = 3$ mice, mean ± SD; ****$p < 0.0001$). (f) and (g) C57BL/6 mice were hypodermic inoculation with 3×10^4 PFU MHV-A59 together with 0.24 μmol (13.2 μg of Mn^{2+}) nanoMn or PBS (vehicle). Fourteen days after the inoculation, the mice were i.p. infected with 3×10^5 PFU MHV-A59. (f) A graphic model of mice treatment. (g) Seven days after the MHV i.p. infection, the inner canthus blood was collected from the infected mice, and subjected to sera immunoglobulin assay ($n = 8$ mice, mean ± SD; ns, not significant: **$p = 0.0086$). (h) Model for the role of nanoMn in host immune response against coronavirus. (b)–(e), and (g) Statistical significance was assessed by two-tailed unpaired Student's *t*-test. (a)–(e), and (g) Data are representative of two independent experiments. See also Fig. S4 in the ESM.

To evaluate the safety of nanoMn, we first examined the distribution of manganese in the mice receiving prior injection of nanoMn or $MnCl_2$. The main organs were collected for determination of Mn^{2+} concentrations by the inductively coupled plasma mass spectrometry (ICP-MS) method. As shown in Figs. S5(a) and S5(b) in the ESM, in contrast to induction of higher Mn^{2+} concentration in spleens (as the major blood storage organ) and serum by $MnCl_2$ treatment, nanoMn treatment leads to higher Mn^{2+} concentration in livers. Moreover, unlike the gradual increase of Mn^{2+} concentration post $MnCl_2$ treatment in brain, nanoMn hardly induced accumulation of Mn^{2+} in CNS (Fig. S5(a) in the ESM). Our data thus indicate that, instead of the engulfment of nanoMn by macrophage, majority of peritoneal $MnCl_2$ were absorbed into blood and subsequently transported into brain.

Previous researches have revealed that the signs of

Mn^{2+}-associated neurotoxicity include production of ROS and increase of pro-inflammatory cytokines in brain [15, 16]. To investigate the neurotoxicity of nanoMn and $MnCl_2$, we performed dihydroethidium (DHE) staining of the brain sections from nanoMn and $MnCl_2$ treated mice. As shown in Fig. S5(c) in the ESM, unlike the increased fluorescence intensity of DHE in the brain treated with $MnCl_2$ 72 h post injection, ROS levels in brains of nanoMn treated mice were stable. Examination of expression levels of pro-inflammatory cytokines associated genes also revealed similar tendency (Fig. S5(d) in the ESM). Moreover, compared with the increase of ALT, LDH and α-HBDH in $MnCl_2$ treated mice, nanoMn treatment hardly influenced the levels of the functional parameters of the liver, kidney and heart (Table S1 in the ESM).

To test whether stimulatory role of nanoMn in interferon response results in inflammation, we assessed the levels of

pro-inflammatory cytokines in livers treated with nanoMn. As shown in Fig. S6(a) in the ESM, compared with virus-induced inflammation, lower level of pro-inflammatory cytokines, such as IL-6 and TNF-α, were induced by nanoMn treatment. Moreover, through analysis of the transcriptome of liver from mice treated with nanoMn, MnCl$_2$, or vehicle, in addition to higher mRNA levels of genes associated with interferon signaling, the pathways associated with metabolism process were hardly affected by nanoMn. Importantly, through limiting viral replication, nanoMn treatment significantly reduced levels of pro-inflammatory cytokines on day 7 post MHV infection (Fig. S6(b) in the ESM). In light of the therapeutic effects of nanoMn in the treatment of coronavirus, our data thus demonstrate that non-toxic nanoMn can be used as a potential drug for the treatment of coronavirus diseases.

3 Discussion

In this study, we have developed a nanoMn that augments host antiviral immune responses, including activation of interferon signaling, induction of M1 macrophage polarization and potentiation of CD8$^+$ T cell memory as well as host adaptive immunity (Fig. 6(h) in the ESM). Moreover, nanoMn greatly decreases the accumulation of manganese in brain, thus avoiding the Mn^{2+}-induced neurotoxicity. All these unique characteristics enable nanoMn as a promising antiviral agent or vaccine adjuvant.

NanoMn is composed of manganese phosphate core and asymmetric lipid bilayer modified with pegylation. The core serves as a nanodepot of bivalent manganese ion while the lipid coating is equally critical for the preparation, stability and even therapeutic outcome of nanoMn. Firstly, the lipid coating is favorable for the preparation of small-size and uniform nanoparticulate manganese. Otherwise, the shape and particle size would be uncontrollable during the process of preparation. Secondly, the lipid bilayers and pegylation guarantee superior stability of nanoMn both *in vitro* and *in vivo*. Naked manganese phosphate without a pegylation hydration layer tends to form aggregates or even precipitations after administration. Although the manganese nanoparticles are preferentially endocytosed by macrophages *in vivo*, the large-scale precipitates of manganese phosphate would be hardly cleared away from the injection site, probably causing potential risk of safety *in vivo*.

We have shown that nanoMn can trigger stronger type-I-IFN response and antiviral effects than free Mn^{2+}. This is mainly attributed to the more efficient cellular uptake of nanoMn and subsequent sustained release of Mn^{2+}. As a nanoparticle, nanoMn is mainly dependent on endocytic pathway for entry into cells [22–24]. Endocytosis of one nanoMn is equivalent to uptake of a large number of free Mn^{2+}. Moreover, the endocytosis pathway does not cause a negative feedback mechanism that typically exists in metal ion transmembrane transporter responsible for entry of free Mn^{2+} into cells [25]. Upon endocytosed by cells, nanoMn persistent releases free Mn^{2+} in the pH-sensitive manner, leading to persistent immune stimulation. All the above characteristics of nanoMn enable extensive interferon productions, particularly attractive for treatment of coronaviruses that induce less production of interferon [9].

The advantage of nanoMn in cellular uptake is further enhanced in macrophages that play dual roles in uptake of nanoparticles and production of type-I-IFN. After preferentially internalized by macrophage, nanoMn further induces M1 macrophage polarization, boosts the production of IFN and facilitates antigen presentation. Moreover, intraperitoneal (i.p.) injection of nanoMn recruits massive monocytes into the inflammatory loci, which may be due to the inflammatory cytokines secreted by the activated macrophages [26, 27]. As the precursor of macrophage, the recruitment of monocytes further strengthens host immune response against viral infection and coordinates viral clearance by adaptive immune system [26, 27]. Above all, the stimulatory effects of nanoMn on host immune response contribute to limitation of viral infection.

SARS-CoV-2 only induces low levels of interferon response and thus fails to promptly clear virus [9]. This is eventually inclined to cause hyper-inflammatory responses with cytokine storm, which plays a major role in inflammatory tissue damage and poor disease prognosis, even death [28]. In this study, nanoMn allows effective clearance of MHV-A59 coronaviruses at the early stage of viral infection, thus ameliorating virus-induced tissue damage and prolonging survival time of the mice. Moreover, nanoMn treatment significantly decreased the production of proinflammatory cytokines in the late stage of viral infection. These results thus highlight the significance of interferon induction at the early stage for treatment of coronavirus infection and potentiality of nanoMn for therapy of COVID-19. The study of nanoMn against SARS-CoV-2 is ongoing.

In addition to boost of IFN production, M1 macrophage polarization by nanoMn can also enhance antigen presentation [21], which indicates that nanoMn holds great promise as a vaccine adjuvant to boost host immune response against pathogens. To avoid the risks associated with live pathogen, the pathogen subunits or other nonliving form of the organism are typically used as the vaccine, whereas the immunogenicity is commonly quite low [29]. The adjuvants are thus employed, which can enhance the immune response and help with delivery of the vaccine to the immune system [30]. For 80 years, the only adjuvant used in human vaccines was aluminum salts [31, 32]. Just like the particle-based strategy we used in this study to change the physical forms of free Mn^{2+} into a controllable nanodepot, albumin salt is also adopted as a type of particulate adjuvant and many other nonmetal emulsions [31–33]. These particulate adjuvants can potentiate innate immune response and ultimately shape the consequences of antibody production through multiple mechanisms such as prolonging release time of immunogenicity, facilitating the formation of large antigen complexes, and so on [31–33]. In our present study, nanoMn treatment can boost host immune response against pathogens. Through triggering the interferon response, nanoMn treatment enhances innate immune response. Moreover, nanoMn treatment polarizes M1 macrophage activation, which acts as antigen-presenting cells, thereby augmenting both cellular and humoral immune response. Importantly, though all of clinical trial or proved adjuvants have been found to enhance the production of antibodies, few if any actually enhance cellular immunity, especially CD8$^+$ T cell responses, which is essential for immune protection against pathogens [34]. Therefore, the enhancement of nanoMn treatment on the development of CD8$^+$ memory T cells makes nanoMn a strong vaccine adjuvant candidate for coronavirus treatment.

By storage of manganese in the core of integrated nanostructure, nanoMn treatment avoids the neurotoxicity of free Mn^{2+} by limiting neural accumulation of Mn *in vivo*. Preferential uptake by macrophage and difficulty in overcoming the blood–brain-barrier remarkably decrease the accumulation of nanoMn in brain, causing no signs of Mn-induced toxicity like ROS production and pro-inflammatory cytokine secretion. In the meantime, the distribution change of nanoMn does not affect the functional parameters of main organs in vivo. Moreover, the dose of nanoMn we used in this study is comparable with the clinically-available manganese formulations.

Manganese (II) dipyridoxyl diphosphate (Mn-DPDP, also known as Teslascan, Nycomed, Oslo, Norway), a manganese formulation, has been approved by FDA to be used as magnetic resonance imaging (MRI) contrast agent in clinic [35]. This agent is administered intravenously at a dosage of 5 μmol/kg, which is close to the dosage we used in this study (12 μmol/kg through intraperitoneal injection). Overall, nanoMn can serve as a safe strategy as either an antiviral drug or a vaccine adjuvant.

In the previous report, Lv et al. find that, through modulating cGAS-STING signaling, Mn^{2+} is essential for innate immune sensing of tumors, and enhances anti-tumor adaptive immunity [36]. These results support our data that Mn treatment can boost anti-viral adaptive immunity, and manganese formulation can act as vaccine adjuvant. However, Lv et al. use $MnCl_2$ in their study, which has nonspecific distributions and neurotoxicity [36]. Through fabricating the manganese nanodepot, we have addressed the defect of free Mn^{2+}, and delivered manganese into macrophages, thus driving M1 macrophages polarization. Therefore, we believe that nanoMn holds great promise for future clinical translation.

In conclusion, we identify an interferon-activating manganese nanodepot that suppresses coronavirus infection. Without causing acute toxicity to organs, nanoMn treatment limits viral propagation and ameliorates the virus-induced immunopathology *in vivo*. More importantly, nanoMn can function as an efficient vaccine adjuvant to boost host adaptive immunity. Our data thus provide a promising nano-drug for the treatment of coronavirus infection.

4   Materials and methods

4.1   Mice

Irf3$^{-/-}$ mice were gifts from Prof. Fuping You. Six weeks old, sex and age matched C57BL/6 mice were used for animal experiments. The mice were maintained in the specific pathogen-free condition at the Department of Laboratory Animal Science of Peking University Health Science Center, and the protocols of animal experiments were approved by the Ethics Committee of Peking University Health Science Center.

4.2   Antibodies and reagents

The antibodies used in this study were as follow: anti-CD45 (30-F11), anti-CD62L (MEL-14), anti-CD25 (PC61.5), antibody to IFN-γ (88-7314) and antibody to TNF-α (MP6-XT22) (all from eBioscience). Anti-CD3 (17A2), anti-CD11b (M1/70), anti-CD44 (IM7), anti-Gr1 (RB6-8C5), anti-B220 (RA3-6B2) (all from Biolegend). Anti-CD4 (GK1.5), anti-CD8 (53-6.7), anti-F4/80 (BM8.1) (all from Tonbo). H-2Db LCMV gp33 Tetramer-KAVYNFATC (TS-5002-1) (MBL). Anti-GAPDH (IC4) (Sungenebiotech). Anti-IRF7 (A0159), anti-ISG15 (A2416) and anti-IRF3 (A2172) (all from ABclonal).

The following reagents were used in the study: $MnCl_2$ and cyclohexane were ordered from Tongguang Company; phospholipids (DOPA, DOTAP and DSPE-PEG) were purchased from Avanti Polar Lipid. Igepal® CO-520 and triton™ X-100 were obtained from Sigma-Aldrich (St. Louis, MO) without further purification. DHE were from GeneCopoeia. Other reagents were analytical pure. Deionised Milli-Q water was used in experiments.

4.3   Preparation of nanoMn

NanoMn was fabricated by a droplet-confined nanoprecipitation in water-in-oil (w/o) micro-emulsion followed by a thin-film dispersion method. Briefly, 300 μL of 500 mM $MnCl_2$ was added drop by dropping into 15 mL of cyclohexane/Igepal CO-520

(70/30 v/v) solution followed by sonication to form a uniformly-dispersed (w/o) micro-emulsion. A similar phosphate w/o micro-emulsion was formulated by 300 μL of 25 mM Na_2HPO_4 in a separate 15 mL of oil phase. After that, 200 μL of dioleoylphosphatydicacid (DOPA) in chloroform was added to the phosphate phase. The above two solutions were then mixed together for 20 min to enable sufficient reaction. The cyclohexane and surfactant were removed from the mixture by addition of 30 mL of absolute ethanol and centrifugation at 12,000*g* for 20 min. The pellets were collected, washed by ethanol 2–3 times, dissolved in 1 mL of chloroform as MnP core. For further preparation of nanoMn, 100 μL of 10 mM DOTAP/Cholesterol (1:1) and 100 μL of 3 mM DSPE–PEG-2000 were added into the MnP core. After evaporating the chloroform, the residual lipid film was dispersed in 800 μL of 5 mM tris–HCl or PBS (pH 7.4) buffer to form nanoMn.

4.4   *In vitro* characterization of nanoMn

The hydrodynamic diameter and zeta potential of nanoMn were determined by a PSS ZPW388-NICOMP Particle Sizing System using a dynamic light scattering method at room temperature. The morphology and size of nanoMn were observed and photographed by TEM (JEOL174 1200EX). For TEM sample preparation, nanoMn were dropped onto a 300-mesh carbon coated copper grid and then negatively stained with 1% uranium acetate. Samples were then loaded into TEM instrument for acquisition of microscopic pictures.

4.5   *In vitro* release of Mn^{2+} from nanoMn

To examine the pH-sensitive release of Mn^{2+} from nanoMn, we performed an experiment of Mn^{2+} release from nanoMn in various pH conditions. Briefly, about 5 mg of dry nanoMn powders were dispersed in 5 mL of buffer solution with various pH values (4.5, 6.5, and 7.4), which were then shaken at 37 °C with a shaking rate of 40 rpm. At predetermined time points (0, 0.5, 1, 2, 3, 4, and 24 h), 200 μL of sample was withdrawn each time and replaced with the same volume of fresh medium. Each sample was further employed for Mn^{2+} concentration determination by inductively coupled plasma optical emission spectrometry to plot the curve of cumulative Mn^{2+} release.

4.6   NanoMn treatment

For treatment of cultured cells with nanoMn, 10 μM nanoMn was directly added to the culture medium, and the cells were cultured at 37 °C for indicated hours. For *in vivo* treatment of nanoMn in viral infection mice model, the mice were intraperitoneally injected with 12 μmol/kg (660 μg/kg Mn^{2+}) nanoMn. The nanoMn was administrated 24 h before or after viral infection as indicated. For administration of nanoMn as immune adjuvant, 0.24 μmol (13.2 μg Mn^{2+}) nanoMn was mixed with inactivated virus. The mixture was then injected subcutaneously into C57BL/6 mice.

4.7   Viral infection and viral titer quantification

For *in vitro* viral infection, virus at indicated titers were directly added to cultured cells. For *in vivo* viral infection, mice were i.p. injected with MHV-A59 at indicated titers. For immunization, virus was inactivated by heating at 54 °C for 30 min, and the mice were subcutaneous injected with the inactivated virus.

Median tissue culture infective dose (TCID50) test was used to quantify the viral titers of MHV-A59. Briefly, 17Cl-1 cells were seeded in 96-well cell culture plates, and infected with 10-fold serial diluted virus for 48 h. The cells were examined using microscope and the wells with pathological cells were

counted. Reed-Muench method was used to calculate viral titers.

To determine the replication rates of VSV-GFP, cells infected with VSV-GFP were collected, and observed with fluorescence microscope. For quantification of the infection efficiency, the cells were subjected to Flow Cytometry analysis, and the rates of VSV-GFP$^+$ cells were used for statistical analysis.

To determine the infection efficiency of MHV-A59, SEV, HSV, LCMV-ARM, or LCMV-Cl13, the infected cells or tissues were collected, and subjected to qRT-PCR analysis. Expression levels of viral RNAs were assessed, using for statistical analysis.

4.8 Immunoblot analysis

Cultured cells were collected, and lysed by Co-IP lysis buffer containing 150 mM NaCl, 1 mM EDTA, 20 mM Tris-HCl pH 8.0, 10% (v/v) glycerol, 0.5% (v/v) NP40, and Protease inhibitor Cocktail (Roche). The cell lysates were subjected to SDS-PAGE and immunoblot analysis.

4.9 qRT-PCR assay

Cells or tissues were collected, and total RNA were isolated using TRIzol reagents (invitrogen), followed by reverse transcribing with GoScriptTM Reverse Transcription System (Promega). Quantitative real-time PCR was performed using TransStart Top Green qPCRSuperMix (TransGen Biotech) and Applied Biosystems™ 7500 system (ThermoFisher Scientific). All primers used in the study were listed in Table S2 in the ESM.

4.10 Enzyme linked immunosorbent assay (ELISA)

BMDMs were treated as indicated, and the culture medium was collected. Mouse IFN-beta ELISA Kit and Mouse Tumor Necrosis Factor Alpha ELISA Kit (ABclonal) were used for ELISA following the manufacturer's instruction. The average concentration lower than 5 pg/mL was identified as not detected.

4.11 ICP-MS

Mice organs or cell lysates were weighting, and digested with nitric acid. Concentration of Mn^{2+} was assessed using ICP-MS-7800 (Agilent). The instrument settings were listed in Table S3 in the ESM.

4.12 Isolation of peritoneal macrophages

Mice were sacrificed, and the abdominal wall was opened to exposure the peritoneum. The peritoneal cells were isolated through peritoneal cavity lavage with 4 mL of RPMI1640 medium. The cells were cultured at 37 °C for 1 h, and the non-attached cells were removed by washing with complete RPMI1640 medium to purify macrophages. Attached cells (macrophages) were subjected to subsequent experiments.

4.13 Induction of BMDMs

To prepare the L929 medium, L929 cells were seeded in T75 flask, and cultured at 37 °C for 10 days. The culture medium was collected for BMDMs induction.
Femur of C57BL/6 mice was harvested, and the bone marrow was isolated by rinsing with PBS. The red blood cells were lysed using ACK-lysis buffer (0.15 mol/L NH$_4$Cl, 10 mmol/L KHCO$_3$, 0.1 mmol/L Na$_2$EDTA, pH 7.2). After culture at 37 °C for 4 h to remove the attached cells, the bone marrow cells were cultured for 7 days in complete Gibco Dulbecco's

modified eagle medium (DMEM) containing 15% (v/v) L929 medium to induce BMDMs.

4.14 DHE staining

Brains were harvested from mice, and fixed with 4% paraformaldehyde (PFA). The organs were dehydrated using 20% and 30% sucrose solution, and embedded with tissue freezing medium (General Data), freezing at –80 °C. The cryopreserved tissue sections were rewarmed with PBS, and stained with 5 μM DHE at room temperature for 30 min under protection from light. The sections were washed with PBS, and incubated with 4',6-diamidino-2-phenylindole (DAPI). A fluorescence microscope was used to analyze the samples.

4.15 RNA-seq data analysis

The RNA-seq data that support the findings in this study have been deposited in the Sequence Read Archive (SRA) database. SRA accession number is PRJNA638008.

RNA-seq data was analyzed with GSEA. Applications from Broad Institute (http://www.broad.mit.edu/gsea/software/software_index.html) with default parameters and GO gene sets downloaded from the Broad Institute Molecular Signature Database (MSigDB) were used for analysis.

Enrichment analysis was performed using clusterProfiler software with GO database.

4.16 Blood biochemistry test

Blood was collected from anesthetized mice, and the blood was centrifuged at 12,000 rpm for 30 min to isolate the serum. Blood biochemistry test was performed using a BS-180 automatic biochemical analyzer (Mindray) following the manufacturer's instruction.

4.17 H&E staining

Tissues were harvested from mice, and fixed in 10% (v/v) neutral buffered formalin. After paraffin-sectioning, the tissues specimens were subjected to H&E staining.

4.18 Preparation of lymphocytes

Spleens were ground in PBS containing 1% (v/v) fetal bovine serum (FBS) to release the lymphocytes, and the cell suspension was filtered through a 75 μM strainer. To isolate lymphocytes infiltrating in the liver, the tissues were minced, and digested using a digestive buffer containing RPMI1640 medium, 10% (v/v) FBS, 0.5 mg/ml Collagenase D (Roche) and 25 μg/mL DNase I (Sigma) at 37 °C for 30 min. Then a 40%/70% Percoll gradient (GE Healthcare) was used to isolate the cells by centrifuging at 800g for 20 min. Lymphocytes at the inter-layer were collected and counted for further operation.

4.19 Flow cytometry

To perform surface staining, lymphocytes isolated from tissues were per-stained with anti-CD16/32 antibody (Biolegend), and then incubated with specific antibodies for 30 min at room temperature. Flow cytometry analysis was performed using a flow cytometry analyzer (BD Biosciences), and analyzed with FlowJo software.

For intracellular cytokine staining, cells were stimulated with 100 ng/mL PMA and 500 ng/mL ionomycin or 2 μg/mL GP$_{33-41}$ peptide together with GolgiPlug and GolgiStop (BD Biosciences) for 5 h. The cells were washed and fixed with IC Fixation Buffer (Invirtrogen) at 4 °C overnight. Then the cells were

permeabilized using CytoVista™ Permeabilization Buffer (Invirtrogen), and stained with specific anti-cytokine antibodies.

4.20 Sera immunoglobulin assay

The inner canthus blood was collected from the mice, and the serum was isolated through centrifuging at 12,000 rpm for 30 min. The serum was diluted 100,000 times with ddH_2O, and subjected to sera immunoglobulin assay using Mouse IgG/IgM ELISA kit (Jiangsu Kete biotech), following the manufacturer's instruction.

4.21 Statistical analysis

Statistical analysis was performed using Prism GraphPad software v6.01. Log-rank (Mantel–Cox) test was used to analyze the statistical significance of survival curve. Statistical significance between two groups was calculated by unpaired Student's t-test. To analyze difference of three or more means, one or two-way analysis of variance (ANOVA) followed by Tukey's multiple comparisons test was used. $p < 0.05$ was considered significant.

References

[1]   Guan, W. J.; Liang, W. H.; Zhao, Y.; Liang, H. R.; Chen, Z. S.; Li, Y. M.; Liu, X. Q.; Chen, R. C.; Tang, C. L.; Wang, T. et al. Comorbidity and its impact on 1590 patients with COVID-19 in China: A nationwide analysis. *Eur. Respir. J.* **2020**, *55*, 2000547.

[2]   Guan, W. J.; Ni, Z. Y.; Hu, Y.; Liang, W. H.; Ou, C. Q.; He, J. X.; Liu, L.; Shan, H.; Lei, C. L.; Hui, D. S. C. et al. Clinical characteristics of coronavirus disease 2019 in China. *N. Engl. J. Med.* **2020**, *382*, 1708–1720.

[3]   Li, G. D.; De Clercq, E. Therapeutic options for the 2019 novel coronavirus (2019-nCoV). *Nat. Rev. Drug Discov.* **2020**, *19*, 149–150.

[4]   Pal, M.; Berhanu, G.; Desalegn, C.; Kandi, V. Severe acute respiratory syndrome coronavirus-2 (SARS-CoV-2): An update. *Cureus* **2020**, *12*, e7423.

[5]   Bao, L.; Deng, W.; Huang, B. Y.; Gao, H.; Liu, J. N.; Ren, L. L.; Wei, Q.; Yu, P.; Xu, Y. F.; Qi, F. F. et al. The pathogenicity of SARS-CoV-2 in hACE2 transgenic mice. *Nature* **2020**, *583*, 830–833.

[6]   Graham, R. L.; Donaldson, E. F.; Baric, R. S. A decade after SARS: Strategies for controlling emerging coronaviruses. *Nat. Rev. Microbiol.* **2013**, *11*, 836–848.

[7]   Kim, K. D.; Zhao, J.; Auh, S.; Yang, X. M.; Du, P. S.; Tang, H.; Fu, Y. X. Adaptive immune cells temper initial innate responses. *Nat. Med.* **2007**, *13*, 1248–1252.

[8]   Yang, Z. S.; Du, J.; Chen, G.; Zhao, J.; Yang, X. M.; Su, L. S.; Cheng, G. H.; Tang, H. Coronavirus MHV-A59 infects the lung

and causes severe pneumonia in C57BL/6 mice. *Virol. Sin.* **2014**, *29*, 393–402.

[9]   Ma, S. Q.; Zhang, J.; Wang, Y. S.; Xia, J.; Liu, P.; Luo, H.; Wang, M. Y. Glucocorticoid therapy delays the clearance of SARS-CoV-2 RNA in an asymptomatic COVID-19 patient. *J. Med. Virol.* **2020**, *92*, 2396–2397.

[10]   Shalhoub, S. Interferon beta-1b for COVID-19. *Lancet* **2020**, *395*, 1670–1671.

[11]   Antonelli, G.; Turriziani, O.; Pierangeli, A.; d'Ettorre, G.; Galardo, G.; Pugliese, F.; Mastroianni, C. M.; Scagnolari, C. Type I interferons can be detected in respiratory swabs from SARS-Cov-2 infected patients. *J. Clin. Virol.* **2020**, *128*, 104450.

[12]   Haji Abdolvahab, M.; Mofrad, M. R. K.; Schellekens, H. Chapter eight - interferon beta: From molecular level to therapeutic effects. *Int. Rev. Cell Mol. Biol.* **2016**, *326*, 343–372.

[13]   Kumar, H.; Kawai, T.; Akira, S. Pathogen recognition by the innate immune system. *Int. Rev. Immunol.* **2011**, *30*, 16–34.

[14]   Wang, C. G.; Guan, Y. K.; Lv, M. Z.; Zhang, R.; Guo, Z. Y.; Wei, X. M.; Du, X. M.; Yang, J.; Li, T.; Wan, Y. et al. Manganese increases the sensitivity of the cGAS-STING pathway for double-stranded DNA and is required for the host defense against DNA viruses. *Immunity* **2018**, *48*, 675–687.e7.

[15]   Peres, T. V.; Schettinger, M. R. C.; Chen, P.; Carvalho, F.; Avila, D. S.; Bowman, A. B.; Aschner, M. "Manganese-induced neurotoxicity: A review of its behavioral consequences and neuroprotective strategies". *BMC Pharmacol. Toxicol.* **2016**, *17*, 57.

[16]   Tjalkens, R. B.; Popichak, K. A.; Kirkley, K. A. Inflammatory activation of microglia and astrocytes in manganese neurotoxicity. In *Neurotoxicity of Metals*; Aschner, M.; Costa, L. G., Eds.; Springer: Cham, 2017; pp 159–181.

[17]   Blasius, A. L.; Beutler, B. Intracellular toll-like receptors. *Immunity* **2010**, *32*, 305–315.

[18]   Miao, X. Y.; Leng, X. F.; Zhang, Q. The current state of nanoparticle-induced macrophage polarization and reprogramming research. *Int. J. Mol. Sci.* **2017**, *18*, 336.

[19]   O'Brien, T. R.; Thomas, D. L.; Jackson, S. S.; Prokunina-Olsson, L.; Donnelly, R. P.; Hartmann, R. Weak induction of interferon expression by severe acute respiratory syndrome coronavirus 2 supports clinical trials of interferon-λ to treat early coronavirus disease 2019. *Clin. Infect. Dis.* **2020**, *71*, 1410–1412.

[20]   McNab, F.; Mayer-Barber, K.; Sher, A.; Wack, A.; O'Garra, A. Type I interferons in infectious disease. *Nat. Rev. Immunol.* **2015**, *15*, 87–103.

[21]   Poltavets, A. S.; Vishnyakova, P. A.; Elchaninov, A. V.; Sukhikh, G. T.; Fatkhudinov, T. K. Macrophage modification strategies for efficient cell therapy. *Cells* **2020**, *9*, 1535.

[22]   Yu, H. J.; Zou, Y. L.; Wang, Y. G.; Huang, X. N.; Huang, G.; Sumer, B. D.; Boothman, D. A.; Gao, J. M. Overcoming endosomal barrier by amphotericin B-loaded dual pH-responsive PDMA-*b*-PDPA micelleplexes for siRNA delivery. *ACS Nano* **2011**, *5*, 9246–9255.

[23]   Smith, S. A.; Selby, L. I.; Johnston, A. P. R.; Such, G. K. The endosomal escape of nanoparticles: Toward more efficient cellular delivery. *Bioconjugate Chem.* **2019**, *30*, 263–272.

[24]   Lin, W.; Vann, D. R.; Doulias, P. T.; Wang, T.; Landesberg, G.; Li, X. L.; Ricciotti, E.; Scalia, R.; He, M.; Hand, N. J. et al. Hepatic metal ion transporter ZIP8 regulates manganese homeostasis and manganese-dependent enzyme activity. *J. Clin. Invest.* **2017**, *127*, 2407–2417.

[25]   Horning, K. J.; Caito, S. W.; Tipps, K. G.; Bowman, A. B.; Aschner, M. Manganese is essential for neuronal health. *Annu. Rev. Nutr.* **2015**, *35*, 71–108.

[26]   Ginhoux, F.; Jung, S. Monocytes and macrophages: Developmental pathways and tissue homeostasis. *Nat. Rev. Immunol.* **2014**, *14*, 392–404.

[27]   Shi, C.; Pamer, E. G. Monocyte recruitment during infection and inflammation. *Nat. Rev. Immunol.* **2011**, *11*, 762–774.

[28]   Catanzaro, M.; Fagiani, F.; Racchi, M.; Corsini, E.; Govoni, S.; Lanni, C. Immune response in COVID-19: Addressing a pharmacological challenge by targeting pathways triggered by SARS-CoV-2. *Signal Transduct. Target. Ther.* **2020**, *5*, 84.

[29]   Stauffer, F.; El-Bacha, T.; Da Poian, A. Advances in the development of

inactivated virus vaccines. *Recent Patents Anti-Infect. Drug Discov.* **2006**, *1*, 291–296.

[30] Reed, S. G.; Orr, M. T.; Fox, C. B. Key roles of adjuvants in modern vaccines. *Nat. Med.* **2013**, *19*, 1597–1608.

[31] Griesenauer, R. H.; Kinch, M. S. An overview of FDA-approved vaccines & their innovators. *Expert Rev. Vaccines* **2017**, *16*, 1253–1266.

[32] HogenEsch, H.; O'Hagan, D. T.; Fox, C. B. Optimizing the utilization of aluminum adjuvants in vaccines: You might just get what you want. *NPJ Vaccines* **2018**, *3*, 51.

[33] Mascola, J. R.; Fauci, A. S. Novel vaccine technologies for the 21st century. *Nat. Rev. Immunol.* **2020**, *20*, 87–88.

[34] Li, X.; Wang, X. P.; Ito, A. Tailoring inorganic nanoadjuvants towards next-generation vaccines. *Chem. Soc. Rev.* **2018**, *47*, 4954–4980.

[35] Karlsson, J. O. G.; Ignarro, L. J.; Lundström, I.; Jynge, P.; Almén, T. Calmangafodipir [$Ca_4Mn(DPDP)_5$], mangafodipir (MnDPDP) and MnPLED with special reference to their SOD mimetic and therapeutic properties. *Drug Discov. Today* **2015**, *20*, 411–421.

[36] Lv, M. Z.; Chen, M. X.; Zhang, R.; Zhang, W.; Wang, C. G.; Zhang, Y.; Wei, X. M.; Guan, Y. K.; Liu, J. J.; Feng, K. C. et al. Manganese is critical for antitumor immune responses via cGAS-STING and improves the efficacy of clinical immunotherapy. *Cell Res.* **2020**, *30*, 966–979.